

# Generation of Alfvénic Waves and Turbulence in Reconnection Jets

Masahiro Hoshino,<sup>1</sup> Katsuaki Higashimori,<sup>1</sup>

**Abstract.** The magnetohydrodynamic linear stability with the localized bulk flow oriented parallel to the neutral sheet is investigated, by including the Hall effect and the guide magnetic field. We observe three different unstable modes: a “streaming tearing” mode at a slow flow speed, a “streaming sausage” mode at a medium flow speed, and a “streaming kink” mode at a fast flow speed. The streaming tearing and sausage modes have a standard tearing mode-like structure with symmetric density fluctuations in the neutral sheet, while the kink mode has an asymmetric fluctuation. The growth rate of the streaming tearing mode decreases with increasing magnetic Reynolds number, while the growth rates of the sausage and kink modes do not depend strongly on the Reynolds number. The sausage and kink modes can be unstable for not only super-Alfvénic flow but also sub-Alfvénic flow when the lobe density is low. The wavelengths of these unstable modes are of the same order of magnitude as the thickness of the plasma sheet. Their maximum growth rates are higher than that of a standard tearing mode, and under a strong guide magnetic field, the growth rates of the sausage and kink modes are enhanced, while under a weak guide magnetic field, they are suppressed. For a thin plasma sheet with the Hall effect, the fluctuations of the streaming modes can exist over the plasma sheet. These unstable modes may be regarded as being one of the processes generating Alfvénic turbulence in the plasma sheet during magnetic reconnection.

## 1. Introduction

Alfvénic fluctuations and turbulence with orders of magnitude from several tens  $R_E$  down to ion inertia lengths are often observed in the earth’s magnetotail [e.g., *Russell*, 1972; *Hoshino et al.*, 1994; *Bauer et al.*, 1995; *Zelenyi et al.*, 2014]. The amplitude of these wave fluctuations in the plasma sheet can reach up to half the value of the lobe magnetic field, and these waves can carry a significant fraction of the plasma energy in the plasma sheet [e.g., *Borovsky et al.*, 1997]. It has been discussed that turbulence with a large wave energy density plays an important role in the transport of mass and momentum in the magnetotail [e.g., *Borovsky and Funsten*, 2003; *Zimbardo et al.*, 2010]. Understanding the effects of this turbulence is believed to be a key factor in obtaining an overall understanding of the various plasma phenomena that occur both in space, and also in astrophysical plasmas [e.g., *Birn et al.*, 2012; *Lazarian et al.*, 2012].

To date, many researchers have discussed the importance of turbulence in the plasma sheet in the context of magnetic reconnection. It has been argued that turbulence plays a crucial role in the dynamic evolution of magnetic reconnection and that the magnetic energy dissipation rate can be enhanced by turbulence [e.g., *Matthaeus and Lamkin*, 1986; *Lazarian and Vishniac*, 1999; *Loureiro et al.*, 2009; *Higashimori et al.*, 2013; *Yokoi et al.*, 2013]. In addition to its role in the dynamic evolution of reconnection, turbulence is believed to play an essential role not only in thermal plasma heating but also in nonthermal particle production through the stochastic scattering of particles [e.g., *Veltri et al.*, 1998; *Greco et al.*, 2002; *Zelenyi et al.*, 1998, 2011; *Lazarian et al.*, 2012]. However, in previous studies, it was postulated that

turbulence can be generated in the high  $\beta$  plasma sheet with a high magnetic Reynolds number, but the detailed mechanism required to generate Alfvénic waves and turbulence during the dynamic evolution of reconnection is not understood as yet.

Several possible candidates for generating Alfvénic fluctuations in the plasma sheet have been proposed: (1) the anisotropic ion beams observed in the plasma sheet boundary layer (PSBL) can generate magnetohydrodynamic (MHD) waves through a family of ion–ion beam instabilities [e.g., *Gary*, 1991; *Krauss-Varban and Omid*, 1995; *Grigorenko et al.*, 2011]. The excited Alfvénic wave in the boundary may penetrate into the plasma sheet because the refractive index of the Alfvén wave in the plasma sheet is higher than in the lobe plasma region. (2) An elongated magnetic diffusion region with strong electric currents may make the tearing mode unstable, and many small-scale plasmoids created by the tearing mode instability can emanate from the diffusion region [e.g., *Loureiro et al.*, 2007; *Samtaney et al.*, 2009; *Bhattacharjee et al.*, 2009; *Pucci and Velli*, 2014]. (3) The magnetic field pile-up region, where the reconnection jet stops suddenly, is expected to excite various plasma waves by releasing the bulk flow energy [e.g., *Hoshino et al.*, 1998, 2001]. In dawn-dusk direction parallel to the electric current, the interchange instability can be excited, because the gradient of the plasma density is opposite to the decelerating plasma flow profile. [e.g., *Nakamura et al.*, 2002; *Lapenta and Bettarini*, 2011]. (4) Turbulence in the solar wind may penetrate into the magnetotail across the magnetopause. Even if the magnetosphere is encircled by a closed magnetic field line, fluctuations in the magnetosonic waves can propagate perpendicular to the magnetic field. (5) In addition to the above possible origins of Alfvénic fluctuations, a reconnection jet at Alfvénic speed can be a free energy source for the MHD instability from the release of bulk flow energy.

In this paper, we focus on an MHD instability triggered by a bulk flow plasma in the reconnection downstream, and propagating to the parallel to the bulk flow. In this situation, some reconnection simulations using the hybrid codes

<sup>1</sup>Department of Earth and Planetary Science, The University of Tokyo, Tokyo, Japan

suggested the generation of a kink-type motion of the reconnection exhaust as one of possible origins of turbulence in the plasma sheet [Lottermoser *et al.*, 1998; Arzner and Scholer, 2001; Higashimori and Hoshino, 2012; Liu *et al.*, 2012], and a tearing mode MHD simulation under the localized bulk flow claimed the rapid excitation of the sausage-type fluctuations [Sato and Walker, 1982]. In addition to these nonlinear simulation results, the MHD linear instability with the localized bulk flow oriented parallel to the neutral sheet, which focuses on only the reconnection exhaust, has been extensively investigated by Shigeta *et al.* [1985]; Wang *et al.* [1988]; Lee *et al.* [1988]; Biskamp *et al.* [1998].

In the MHD linear stability analysis, three important modes have been discussed. One of the unstable modes is the “streaming tearing” mode [Shigeta *et al.*, 1985; Wang *et al.*, 1988], categorized as a resistive MHD instability, and a second mode is the “streaming sausage” mode [Lee *et al.*, 1988; Biskamp *et al.*, 1998], categorized as an ideal MHD instability. The eigenfunctions of the streaming tearing/sausage modes are similar to the standard tearing mode [Furth *et al.*, 1963], whose density perturbation is symmetrical to the neutral sheet. The streaming tearing/sausage modes are not zero-frequency modes, and the tearing islands drift with the bulk flow speed. In addition to the two symmetric unstable modes above, an asymmetric unstable mode can be observed, which we call the “streaming kink” mode [Lee *et al.*, 1988; Biskamp *et al.*, 1998]. This mode can be categorized as an ideal MHD instability, and has an instability mechanism that is similar to the streaming sausage mode. (Note that the terminology of the drift-kink instability whose mode is propagating along the electric current direction is different from the streaming kink instability discussed in this paper [Pritchett *et al.*, 1996; Zenitani and Hoshino, 2005; Fujimoto, 2011].)

In this paper, using the standard method of matrix eigenvalue analysis, we studied the above three different types of streaming modes from sub-Alfvénic to super-Alfvénic regime, by paying special attention to the earth’s magnetotail where the lobe density is low, because the dependence of bulk flow speed on the linear growth rate has not been systematically investigated, and because the dilute lobe plasma environment has not been taken into account. We observed that the streaming sausage and streaming kink modes became unstable in the magnetotail when the bulk flow speed reaches a value of several tens of percent of the Alfvén speed. More importantly, we studied the streaming modes under the effects of the Hall current and the guide magnetic field, and propose a possible origin of turbulence in the plasma sheet during magnetic reconnection. In Section 2, the basic model is described with a bulk flow plasma in the center of the plasma sheet, and we introduce the method used to solve the linear stability of the streaming plasmas. In Section 3, we discuss our linear stability results for both the streaming tearing/sausage modes and the streaming kink mode. In Section 4, we summarize our results and provide a perspective on the streaming instabilities.

## 2. Streaming Plasma Sheet Model and Linear Analysis

In this paper, we discuss the streaming MHD modes in the framework of the Hall MHD. As discussed later, the streaming instability itself can be activated in the standard MHD regime without the Hall effect, but we use the Hall MHD equation having its application to the earth’s magnetotail in mind, because from satellite observations, the thickness of the reconnection region is known to be of the order of the ion inertial length [e.g., Sergeev *et al.*, 1993; Asano *et al.*, 2003; Nakamura, 2006].

We studied the linear stability of a Harris-type plasma sheet with a finite bulk flow oriented parallel to an antiparallel magnetic field. The initial equilibrium state was set to

the Harris solution, where the magnetic field  $B_x$  is given by

$$B_x = B_{\text{lobe}} \tanh(y/\lambda), \quad (1)$$

and  $B_y = 0$  and  $B_z = \text{const.}$ , where  $\lambda$  is the thickness of the plasma sheet. The plasma density,  $\rho$ , is expressed by

$$\rho = \frac{\rho_{\text{ps}}}{\cosh^2(y/\lambda)} + \rho_{\text{lobe}}. \quad (2)$$

In this paper, we assumed a finite background density,  $\rho_{\text{lobe}}$ , exists over the entire plasma sheet. The temperature for the uniform component,  $\rho_{\text{lobe}}$ , was assumed to be  $T_{\text{lobe}} = 0$ .

In addition to the standard Harris state, we added a finite bulk flow, whose velocity profile,  $v_x$ , is given by

$$v_x = \frac{v_{\text{jet}}}{\cosh^2(y/\lambda_{\text{jet}})}, \quad (3)$$

and  $v_y = v_z = 0$ , where  $\lambda_{\text{jet}}$  is the thickness of the bulk flow. The bulk flow may mimic the reconnection exhaust with an Alfvénic jet. An MHD instability coupled with the streaming plasma may be activated because of this streaming plasma.

We used a set of compressible MHD equations

$$\frac{\partial \rho}{\partial t} = -\nabla \cdot (\rho \vec{v}), \quad (4)$$

$$\frac{\partial \vec{v}}{\partial t} + \vec{v} \cdot \nabla \vec{v} = -\frac{1}{\rho} \nabla p + \frac{1}{\rho c} \vec{j} \times \vec{B} + \nu \nabla^2 \vec{v}, \quad (5)$$

$$\frac{\partial \vec{B}}{\partial t} = \nabla \times (\vec{v} \times \vec{B} - \frac{1}{en} \vec{j} \times \vec{B}) + \eta \nabla^2 \vec{B}, \quad (6)$$

where the terms  $e$  and  $n$  in the  $\vec{j} \times \vec{B}$  Hall component represent the electric charge and the number density, respectively. The equation of state is assumed to be adiabatic, i.e.,  $p \propto \rho^\gamma$ , where the ratio of the specific heat is  $\gamma = 5/3$ . The electron temperature was set to zero. The terms  $\nu$  and  $\eta$  are the fluid viscosity and the electric resistivity, respectively.

After linearizing the above equations using the standard perturbation method in  $x$  and  $y$  two-dimensional space, we solved the set of linearized equations using the matrix eigenvalue method, which is often used in the analysis of plasma instabilities [e.g., Hoshino, 1991]. The time derivative,  $\partial f(x, y, t)/\partial t$ , of the physical quantity,  $f$ , and the spatial derivative along the plasma sheet,  $\partial f(x, y, t)/\partial x$ , can be expressed by  $-i\omega f(k, y, \omega)$  and  $ik\tilde{f}(k, y, \omega)$  using a Fourier–Laplace transformation in time and space, respectively. In this paper, we assumed that the physical quantities were uniform in the  $z$  direction, i.e.,  $\partial/\partial z = 0$ .

The spatial derivatives in the direction vertical to the plasma sheet,  $\partial f/\partial y$ , can be approximated by the fourth-order, finite difference representation of the differentiation with respect to  $y$ . In addition to this, we used a nonuniform grid spacing. For example, the first derivative in the finite difference representation  $\partial f/\partial y$  can be expressed by

$$\frac{\partial f(x, y_i, t)}{\partial y} = \sum_{j=-2}^2 a_j f(x, y_{i+j}, t), \quad (7)$$

where  $y_i$  is the position of  $i$ -th grid, and

$$a_{i\pm 2} = \pm \frac{\Delta_{i\pm 1} \Delta_{i\mp 1} \Delta_{i\mp 2}}{\Delta_{i\pm 2} (\Delta_{i\mp 2} + \Delta_{i\pm 2}) (\Delta_{i\pm 1} - \Delta_{i\pm 2}) (\Delta_{i\mp 1} + \Delta_{i\pm 2})},$$

$$a_{i\pm 1} = \pm \frac{\Delta_{i\pm 2} \Delta_{i\mp 1} \Delta_{i\mp 2}}{\Delta_{i\pm 1} (\Delta_{i\mp 1} + \Delta_{i\pm 1}) (\Delta_{i\mp 2} + \Delta_{i\pm 1}) (\Delta_{i\pm 2} - \Delta_{i\pm 1})},$$

$$a_i = \frac{\Delta_{i-1} + \Delta_{i-2}}{\Delta_{i-1}\Delta_{i-2}} - \frac{\Delta_{i+1} + \Delta_{i+2}}{\Delta_{i+1}\Delta_{i+2}},$$

where  $\Delta_{i\pm 1} = |y_{i\pm 1} - y_i|$  and  $\Delta_{i\pm 2} = |y_{i\pm 2} - y_i|$ . A nonuniform grid size is useful for resolving the resistive layer in the vicinity of the neutral sheet for the case of a large magnetic Reynolds number [e.g., *Hoshino, 1991*]. The grid size in the vicinity of the neutral sheet was set to be five to 50 times smaller than that in the lobe region. The number of grid points was chosen to be in the range 400 to 1600 to ensure the convergence of the numerical results.

The size of the plasma sheet,  $|y| < L$ , was set to be  $L/\lambda = 5$ , and the boundary condition was assumed to be  $f(x, |y| = L, t) = 0$  for the spontaneous reconnection model. In our study, we used the magnetic Reynolds number,  $R_M = V_A \lambda / \eta = 10^3$ , and the fluid Reynolds number,  $R_V = V_A \lambda / \nu = 10^4$ , in most of our calculations, except for the cases mentioned. The other plasma parameters discussed in this paper are listed in Table 1.

### 3. Results of the Streaming MHD Instability

#### 3.1. Streaming instability with symmetric or asymmetric perturbation

Figures 1a–c show the linear growth rates obtained from our matrix eigenvalue analysis for three different bulk flow speeds. The top of each panel shows the linear growth rate,  $\text{Im}(\omega\tau_A)$ , while the bottom of each panel shows the oscillation frequency,  $\text{Re}(\omega\tau_A)$ , where  $\tau_A = \lambda/V_A$  is the Alfvén transit time. Figure 1a shows the case where there was no bulk flow,  $V_{\text{jet}} = 0$ , and we only obtained the standard tearing mode [*Furth et al., 1963*], where the unstable region only appeared for  $k\lambda < 1$ , and the oscillation frequency was zero.

Figure 1b shows the case for a finite bulk flow speed with  $V_{\text{jet}} = v_{\text{jet}}/V_{A,\text{lobe}} = 0.2$ , normalized to the lobe Alfvén speed, defined by  $V_{A,\text{lobe}} = B_{\text{lobe}}/\sqrt{4\pi\rho_{\text{lobe}}}$ . Note that the bulk flow speed is normalized to the lobe Alfvén speed, while the Alfvén transit time was normalized to the Alfvén speed, defined by the total plasma density in the neutral sheet,  $\rho_0 = \rho_{\text{ps}} + \rho_{\text{lobe}}$ , because the reconnection jet speed was expected to reach to the lobe Alfvén speed when a switch-off shock formed in the boundary.

In Figure 1b, it can be seen that the unstable region extended to the larger wave number region for  $k\lambda > 1$ , and that the growth rate was enhanced slightly compared with the standard tearing mode in Figure 1a. The oscillation frequency,  $\text{Re}(\omega\tau_A)$ , denoted by the red-colored circles can be approximated by the drift frequency/Doppler shift frequency of  $\text{Re}(\omega\tau_A) \simeq (k\lambda)V_{\text{jet}}$ , depicted by the black curve. We confirmed that the behavior of the linear growth rate was basically the same as the “streaming tearing” mode studied by *Shigeta et al. [1985]*; *Wang et al. [1988]*, and we found that from the eigenfunctions the density perturbation was symmetric to the neutral sheet (not shown here).

Figure 1c shows the growth rate and the oscillation frequency for a higher bulk flow speed with  $V_{\text{jet}} = v_{\text{jet}}/V_{A,\text{lobe}} = 0.4$ . In addition to the streaming tearing mode denoted by the red-colored circles, we observed the streaming kink mode, denoted by the green-colored squares, whose density perturbation,  $\rho$ , and vector potential,  $A_z$ , became asymmetric versus the neutral sheet. The streaming kink mode could not be excited below a given minimum threshold speed. However, since the threshold speed was less than the lobe Alfvén velocity,  $V_{A,\text{lobe}}$ , the streaming kink mode can be easily generated during magnetic reconnection. Another interesting point is that the growth rate of the streaming kink mode was larger than the streaming tearing mode, and the streaming kink mode may dominate the plasma sheet turbulence in the reconnection jet.

Figure 2 shows typical linear structures of the vector potential,  $A_z$ , and plasma density,  $\rho$ , in  $(x, y)$  space that were reconstructed from the eigenvalues and eigenfunctions

in Fourier  $(k, y)$  space. The first-order perturbations were superposed onto the zero-order quantities, and we assumed the magnitude of the first-order peak density was 30% of the zero-order density in the neutral sheet. Figure 2a shows the streaming tearing mode for  $(V_{\text{jet}}, k\lambda) = (0.2, 0.3)$ ; Figure 2b shows the streaming kink mode for  $(V_{\text{jet}}, k\lambda) = (0.4, 1.5)$ . The structure of the streaming tearing mode was similar to that of the standard tearing mode, except for the magnetic islands that streamed with the zero-order bulk flow speed,  $v_{\text{jet}}$ . On the other hand, the structure of the streaming kink mode had a periodic distortion in the neutral sheet.

#### 3.2. Maximum growth rate

So far, we have discussed that the streaming tearing mode is unstable for a relatively slow bulk flow regime, while the streaming kink mode appears to be unstable in a relatively fast flow regime. Let us now study the behavior of the two unstable modes as a function of the bulk flow speed,  $V_{\text{jet}}$ .

Figure 3 shows the maximum growth rate and the corresponding wave number as a function of the bulk flow speed,  $V_{\text{jet}}$ . In our numerical calculations, we surveyed the growth rate and the oscillation frequency for a given wave number for  $k\lambda = 0.05 \times i$ , for  $i = 0$  to 63. The wave number and bulk flow were normalized to the thickness of the plasma sheet,  $\lambda$ , and the lobe Alfvén velocity,  $V_{A,\text{lobe}}$ , respectively. The red-colored circles denote the streaming tearing mode, while the green-colored circles denote the streaming kink mode. We observed that the streaming tearing mode with a symmetric density perturbation dominated the regime where  $V_{\text{jet}} < 0.4$ , while the growth rate of the streaming kink mode became larger than that of the streaming tearing mode when the bulk flow speed exceeded about  $V_{\text{jet}} > 0.4$ . These modes have a long wavelength nature for  $k\lambda < 2$ .

By carefully examining the streaming tearing mode denoted by the red-colored circles, we could observe that the characteristics of the unstable wavelengths were different below and above a value of  $V_{\text{jet}} \sim 0.25$ . The unstable wavelengths for  $V_{\text{jet}} < 0.25$  were the long wavelengths with  $k\lambda < 1$ , while for  $V_{\text{jet}} > 0.25$ , the unstable wavelengths occurred for  $1 < k\lambda < 2$ . Moreover, the growth curve of  $\text{Im}(\omega\tau_A)$  showed a discontinuous transition from  $\text{Im}(\omega\tau_A) \sim 10^{-2}$  to  $5 \times 10^{-2}$  around a value of  $V_{\text{jet}} \sim 0.25$ . This suggests that two different modes may exist below and above  $V_{\text{jet}} \sim 0.25$ .

As we discuss this behavior further in the next subsection, 3.3, it can be approximated that the linear growth rate of the symmetric unstable mode for  $V_{\text{jet}} < 0.25$  strongly depends on the magnetic Reynolds number, while the linear growth rate of the symmetric unstable mode for  $V_{\text{jet}} > 0.25$  does not depend on the magnetic Reynolds number. Therefore, we distinguish the symmetric perturbations from their dependence of the linear growth rate on the magnetic Reynolds number,  $R_M$ . One of these modes is the “streaming tearing” mode, categorized as a resistive MHD mode [*Shigeta et al., 1985*; *Wang et al., 1988*], and the other mode is the “streaming sausage” mode, classified as an ideal MHD mode [*Lee et al., 1988*; *Biskamp et al., 1998*]. The streaming tearing and streaming sausage modes are observed in relatively slow and fast bulk flow speeds, respectively.

The perturbed structure of the streaming sausage mode is similar to that of the streaming tearing mode (not shown here), and the vector potential,  $A_z$ , and the plasma density,  $\rho$ , for the streaming tearing/sausage modes show similar properties to the standard tearing mode, namely those perturbations are symmetric against the neutral sheet.

#### 3.3. Reynolds number dependence, $R_M$

Figure 4 shows the linear growth rates for the streaming tearing, streaming sausage, and streaming kink modes as a function of the magnetic Reynolds number. The bulk flow speed was fixed to be  $V_{\text{jet}} = 0.5$  for all cases. The red-colored circles with the solid line and the red-colored circles with the dashed line denote the growth rates of the symmetric density perturbation for the streaming tearing mode with  $k\lambda = 0.3$  and the streaming sausage mode with  $k\lambda = 1.0$ , respectively. The green-colored squares correspond to the streaming kink mode with an asymmetric density perturbation for the wave number with  $k\lambda = 1$ . There may be more than one unstable mode for any given wave number. The streaming sausage and streaming kink modes showed symmetric and asymmetric density fluctuations, respectively.

The growth rate of the streaming tearing mode decreased with increasing magnetic Reynolds number,  $R_M$ , and the growth rate was approximately  $\text{Im}(\omega\tau_A) \propto R_M^{-1/3}$ , which showed a similar dependence to that of the standard tearing mode of  $R_M^{-3/5}$  [Furth *et al.*, 1963], in the sense that it was a decreasing function. The streaming tearing mode is slightly enhanced for a large magnetic Reynolds number, by utilizing the free energy of the streaming bulk flow. On the other hand, the growth rate of the streaming sausage and streaming kink modes did not depend strongly on the Reynolds number, and the growth rates were almost constant in the high magnetic Reynolds number regime. This result is consistent with the streaming sausage and streaming kink modes under an ideal MHD regime discussed by Lee *et al.* [1988]; Biskamp *et al.* [1998]. Therefore, in a plasma medium with a high magnetic Reynolds number,  $R_M$ , the streaming sausage and streaming kink modes may play an important role in the excitation of Alfvénic fluctuations, even if the streaming tearing mode cannot be excited.

### 3.4. Lobe density dependence, $\rho_{\text{lobe}}/\rho_0$

We confirmed that the streaming tearing/sausage and streaming kink instabilities can be excited by adding a bulk flow plasma to the plasma sheet [e.g., Shigeta *et al.*, 1985; Wang *et al.*, 1988; Lee *et al.*, 1988; Biskamp *et al.*, 1998], and these instabilities are thought to be important in the reconnection jet region. Since the reconnection jet speed is known to be the lobe Alfvén velocity if a switch-off slow mode shock is formed, the generation of turbulence by the streaming instabilities may be strongly controlled by the lobe plasma density.

To study the dependence of the lobe plasma density on the linear stability, the data in Figure 5 show the growth rate for  $\rho_{\text{lobe}}/\rho_0 = 0.01, 0.05$ , and  $0.1$ , where  $\rho_0 = \rho_{\text{ps}} + \rho_{\text{lobe}}$  is the total plasma density in the neutral sheet [e.g., Ishisaka *et al.*, 2001]. Figure 5a shows the same data as in Figure 3. It can be seen that the streaming tearing and streaming sausage modes with a symmetric perturbation are excited in the relatively slow bulk flow regime, while the streaming kink mode with an asymmetric perturbation appears in a relatively fast flow regime. The onset speeds of the streaming sausage and kink modes increased with increasing lobe plasma density,  $\rho_{\text{lobe}}/\rho_0$ .

Discontinuous features in the growth rates of the symmetric perturbation, suggesting a transition from the streaming tearing mode to the streaming sausage mode, were observed around  $V_{\text{jet}} \sim 0.25, 0.55$ , and  $0.75$  for  $\rho_{\text{lobe}}/\rho_0 = 0.01, 0.05$ , and  $0.1$ , respectively. The onset speed of the transition also increased with increasing the lobe plasma density. The growth rates for the streaming tearing and streaming sausage modes did not change appreciably on increasing the lobe plasma density, but growth rates for the streaming kink mode could be suppressed because of the contribution of the dense lobe plasma.

Let us now look at the detail on the streaming tearing mode. We can recognize modest peaks in the growth rates for relatively small jet velocities, namely the positions of

the peaks are  $V_{\text{jet}} \sim 0.1$  for  $\rho_{\text{lobe}}/\rho_0 = 0.01$ ,  $V_{\text{jet}} \sim 0.2$  for  $\rho_{\text{lobe}}/\rho_0 = 0.05$ , and  $V_{\text{jet}} \sim 0.3$  for  $\rho_{\text{lobe}}/\rho_0 = 0.1$ . We find these peaks almost correspond to the sound speeds in the plasma sheet,  $c_s = \sqrt{\gamma T_{\text{ps}} \rho_{\text{ps}} / \rho_0}$ , which are  $c_s/V_{A, \text{lobe}} = 0.091, 0.204$ , and  $0.289$  for  $\rho_{\text{lobe}}/\rho_0 = 0.01, 0.05$ , and  $0.1$ , respectively. The streaming tearing mode can be amplified in the subsonic jet flow, while it can be suppressed in the supersonic jet flow.

The reason why the growth rate of the streaming tearing instability is enhanced in the subsonic flow may be interpreted from the decrease in gas pressure around the X-type point, and the resulting emission of a fast expansion wave. The streaming plasma around the X-type point can be squeezed by the reconnecting magnetic field lines, and as a result, the streaming plasma speed can increase. Based on Bernoulli's principle of the dynamic and gas pressure balance along a streamline with  $\rho v^2/2 + p = \text{const.}$ , the gas pressure decreases, and the inflow plasma toward the X-type region can be enhanced. On the other hand, for the case of a supersonic flow, the streaming plasma flowing around the squeezed X-type point can be decelerated, and then the gas pressure increases. Therefore, the inflow of plasma toward the X-type point can be suppressed.

A transition from streaming tearing to streaming sausage modes was observed around  $V_{\text{jet}} = 0.25, 0.55$ , and  $0.75$  for  $\rho_{\text{lobe}}/\rho_0 = 0.01, 0.05$ , and  $0.1$ , respectively. The streaming sausage and streaming kink modes are classified as nonresistive MHD instabilities, and the mechanism of the instability may be controlled by the balance between the tension force of the magnetic field and the centrifugal force of the bulk flow under an infinitesimal distorted magnetic field line. If the bulk flow speed is fast enough to overcome the tension force of the magnetic field line, then we expect the streaming sausage and streaming kink instabilities to occur. Let us assume that the distortion of the magnetic field lines occurs at the boundary between the lobe and the plasma sheet at  $y = \alpha \lambda_{\text{jet}}$ , where  $\alpha \sim 1$  is a tuning parameter determined by the details of the plasma process. Then, the marginal state of the instability can be expressed by

$$\frac{B_{\text{lobe}}^2 \tanh^2(\alpha')}{4\pi} = \left( \frac{\rho_{\text{ps}}}{\cosh^2(\alpha')} + \rho_{\text{lobe}} \right) \frac{v_{\text{jet}}^2}{\cosh^4(\alpha)}, \quad (8)$$

where  $\alpha' = \alpha \lambda_{\text{jet}}/\lambda$ . In this case, the onset velocity of the streaming sausage may be given by

$$V_{\text{jet}} = \cosh^2(\alpha) \tanh(\alpha') / \sqrt{1 + \frac{1}{\cosh(\alpha')^2} \frac{\rho_{\text{ps}}}{\rho_{\text{lobe}}}}. \quad (9)$$

For  $\alpha = \alpha' = 0.96$  with  $\lambda_{\text{jet}} = \lambda$ , we obtain  $V_{\text{jet}} = 0.25, 0.54$ , and  $0.75$  for  $\rho_{\text{lobe}}/\rho_0 = 0.01, 0.05$ , and  $0.1$ , respectively. This simple estimation can model all the transition velocities from the streaming tearing to the streaming sausage modes very well.

The transition from the streaming sausage mode to the streaming kink mode, which can be recognized by the change in symbol from the red-colored circles to the green-colored squares in Figure 5, appears around  $V_{\text{jet}} = 0.4, 0.8$ , and  $1.05$  for  $\rho_{\text{lobe}}/\rho_0 = 0.01, 0.05$ , and  $0.1$ , respectively. These transition velocities can be modeled by assuming  $\alpha = 1.1$  in Eq. (9), and again, we obtain  $V_{\text{jet}} = 0.36, 0.80$ , and  $1.08$  for  $\rho_{\text{lobe}}/\rho_0 = 0.01, 0.05$ , and  $0.1$ , respectively.

In the earth's magnetotail, the lobe plasma density is lower than the plasma sheet density, i.e.,  $\rho_{\text{lobe}}/\rho_{\text{ps}} \sim 0.01 - 0.05$  [e.g. Ishisaka *et al.*, 2001]. On the other hand, many MHD simulation studies of magnetic reconnection assume a relatively higher plasma density exists in the lobe to reduce the Alfvén velocity and to save on computational CPU time. A high density plasma can suppress the emission of

the streaming kink instability, and this may be one reason why no streaming kink instability in association with MHD magnetic reconnection simulations has been reported.

### 3.5. Effect of bulk flow size, $\lambda_{\text{jet}}$

It is also of interest to study the effect of the jet size  $\lambda_{\text{jet}}$ , because the free parameter  $\lambda_{\text{jet}}$  is independent of the equilibrium state. Figure 5d shows the result where  $\lambda_{\text{jet}} = 0.5$ , but keeping  $\rho_{\text{lobe}}/\rho_0 = 0.1$ , the same as in Figure 5c. By comparing Figures 5c and 5d, we find that the growth rate of the streaming tearing mode can be enhanced in the range  $V_{\text{jet}} < 0.25$ , namely almost in the subsonic flow regime, and is reduced in the supersonic flow regime, where the sound speed is  $c_s/V_{A,\text{lobe}} = 0.289$ . The enhancement and suppression of the growth rate is much magnified in the case of Figure 5d. The reason for this is probably because of the localization of the instability inside the high  $\beta$  plasma sheet, where the magnetic field is weak. That is, for the case of a narrow jet, the instability appears close to the neutral sheet with a weak magnetic field, and the effect of the magnetic tension/pressure becomes less important compared with the plasma dynamic and gas pressures.

The onset velocity of the streaming sausage and streaming kink modes for a narrow jet is reduced compared with Figure 5c. This can also be interpreted by the weak magnetic field tension force. By using the modeling of the onset jet velocities in Eq. (9) with the same values of  $\alpha = 0.96$  and  $\alpha' = 0.96(\lambda_{\text{jet}}/\lambda) = 0.48$ , we obtained  $V_{\text{jet}} = 0.45$ , which agrees very well with the onset of the streaming sausage mode. For the transition from the streaming sausage mode to the streaming kink mode, by substituting the same value of  $\alpha = 1.1$  and  $\alpha' = 1.1(\lambda_{\text{jet}}/\lambda) = 0.55$ , we obtained  $V_{\text{jet}} = 0.68$ . Again, we obtain a good agreement between the linear analysis and the theoretical modeling.

The enhancement of the linear growth rate can be understood from the localization of the instability in the vicinity of the neutral sheet because of the narrow jet flow. For a distorted magnetic field line, the magnetic tension force becomes weak, while the centrifugal force of the bulk flow remains constant, if the bulk flow speed is constant. Therefore, the linear growth rate can be enhanced by reducing the size of the bulk flow. However, since the total free energy required to excite the streaming instabilities is reduced, the magnitude of the amplitude of the nonlinear saturation of the streaming instabilities may remain small. A discussion of the saturation level is beyond the scope of our linear analysis.

### 3.6. Mode structure under the Hall effect

So far, we have discussed the behavior of the streaming modes by neglecting the Hall effect, that is, we have assumed that the ion inertia length is much smaller than the thickness of the plasma sheet. However, it is known that the thickness of the plasma sheet is of the order of the ion inertia length near the reconnection region. In this subsection, we discuss the effect of the Hall term on the streaming instabilities.

Figure 6 shows the maximum growth rate and its corresponding wave number as a function of the bulk flow speed,  $V_{\text{jet}}$ , under the Hall MHD with  $(V_A/\Omega_i)/\lambda = 1.0$ . The other parameters are the same as those shown in Figure 3 without any Hall effect. By comparing Figures 3 and 6, we find that: (1) the linear growth rate of the Hall tearing mode is larger than that of the standard MHD tearing mode at  $V_{\text{jet}} = 0$ ; (2) regardless of the Hall term, the three different streaming tearing, streaming sausage, and streaming kink modes are separated by bulk flow speeds of  $V_{\text{jet}} \sim 0.2$ , and 0.3; and (3) under a Hall effect, the growth rate does not change much but the unstable region is shifted to slightly longer wavelengths.

Let us now look at the eigenstructure of the streaming modes under the Hall effect shown in Figure 6. Figures 7a–c show the reconstructed structures for  $V_{\text{jet}} = 0, 0.2$ , and

0.4 in the two-dimensional  $x$ – $y$  space, respectively. We have chosen the wave numbers with the maximum growth rate for the fixed bulk jet speed, namely  $k\lambda = 0.25, 0.5$ , and  $0.5$  for  $V_{\text{jet}} = 0, 0.2$ , and  $0.4$ , respectively. The reconstructed structures were obtained by superposing the first-order perturbations onto the zero-order quantities, and we assumed the magnitude of the first-order peak density was 30% of the zero-order peak density in the neutral sheet.

In Figure 7 (a), the quadrupole magnetic field structure  $B_z$  from the Hall effect can be seen to be localized in the vicinity of the neutral sheet. Note that we assumed a magnetic Reynolds number of  $R_M = 10^3$ , but a lower value of  $R_M$  can produce a wider quadrupole magnetic field structure. By increasing the bulk flow speed up to (b)  $V_{\text{jet}} = 0.2$  and (c)  $V_{\text{jet}} = 0.4$ , in addition to the localized  $B_z$  component in the vicinity of the neutral sheet, large-scale fluctuations outside the localized  $B_z$  component for both the streaming sausage mode and the streaming kink mode were clearly seen. The polarity of  $B_z$  is asymmetric for the streaming sausage mode and symmetric for the streaming kink mode. In association with the generation of  $B_z$ , the global plasma flow pattern in the entire plasma sheet can be seen, as recognized from the white arrows in the vertical direction. We believe that the Hall term may have a significant effect on the generation of Alfvénic fluctuations in the plasma sheet.

### 3.7. Guide magnetic field effect

It is also interesting to study the effect of the guide magnetic field  $B_z$  on the streaming instabilities, because a global dynamical behavior of magnetic reconnection is known to be controlled by the guide magnetic field. In fact, the guide magnetic field in the magnetotail, which is the dawn-dusk magnetic field, is known to exist due to the penetration of the solar wind magnetic field [e.g., Cowley, 1981; Petrukovich, 2011; Rong et al., 2012].

Shown in Figure 8 is the growth rates of the standard tearing mode and the streaming tearing, sausage and kink modes as a function of the initial guide magnetic field  $B_z$ . The guide magnetic field is normalized by the lobe magnetic field  $B_{\text{lobe}}$ , and the growth rate is normalized by the Alfvén transit time. The growth rate of the standard tearing mode with  $(k\lambda, V_{\text{jet}}) = (0.3, 0)$  denoted by the blue-solid line does not depend on the magnitude of the guide magnetic field, and that of the streaming tearing mode with  $(k\lambda, V_{\text{jet}}) = (0.3, 0.8)$  denoted by the blue-dashed line slightly increases as increasing the guide magnetic field. However, the streaming sausage and kink modes with the shorter wavelengths show significant change on the guide magnetic field. The red-solid and red-dashed lines show respectively the sausage mode with  $(k\lambda, V_{\text{jet}}) = (1.0, 0.8)$  and  $(k\lambda, V_{\text{jet}}) = (1.5, 0.8)$ , while the green-solid and green-dashed lines are the kink mode with  $(k\lambda, V_{\text{jet}}) = (1.0, 0.8)$  and  $(k\lambda, V_{\text{jet}}) = (1.5, 0.8)$ , respectively. These sausage and kink modes have a tendency to be stabilized for a relatively weak guide magnetic field  $B_z/B_{\text{lobe}} < 0.5$ , while they are destabilized for a large guide magnetic field  $B_z/B_{\text{lobe}} > 0.5$ .

It should be noted that the inclusion of the guide magnetic field may reduce the plasma compressibility, and that the velocity shear instability such as Kelvin-Helmholtz instability has been shown to be destabilized by a strong vertical magnetic field perpendicular to the shear plasma flow [Miura and Pritchett, 1982]. The similarity of the basic behavior between Kelvin-Helmholtz instability and the streaming sausage and kink instability has been discussed by Lee et al. [1988]; Biskamp et al. [1998], and the incompressible limit due to the strong magnetic field may enhance the growth rates of the streaming sausage and kink instabilities.

## 4. Discussion and Conclusions

We have observed that the streaming MHD instability can be activated by not only a super-Alfvénic bulk flow but also a sub-Alfvénic flow, oriented parallel to the antiparallel magnetic field by taking into account of the dilute plasma environment in the lobe, and found that the growth rates were enhanced more strongly than the standard tearing mode without bulk flow. We also studied that the guide magnetic field perpendicular to the bulk flow can significantly modify the growth rates of the streaming sausage and kink modes. Furthermore, we also found that Alfvénic perturbations of  $B_z$  could be generated outside the plasma sheet when the Hall effect is included. The perturbations may play an important role in the emission of MHD waves over the plasma sheet. We believe that the streaming modes may be a candidate for plasma sheet turbulence.

Since we observed that the bulk flow embedded in the plasma flow could excite three different streaming modes, depending on the bulk flow speed, the next important issue to understand is the nonlinear evolution and the saturation of the instabilities. *Sato and Walker* [1982] investigated the streaming tearing mode using MHD simulations, and suggested that the streaming tearing mode is excited much more in the presence of bulk flow. However, as *Sato and Walker* [1982] assumed that the initial plasma density was uniform over the plasma sheet, they only discussed the streaming tearing mode with a symmetric density perturbation against the neutral sheet. Because a low density plasma in the lobe region is required to excite the kink mode, based on our linear stability analysis, a streaming kink mode was not demonstrated in their simulations. It is important to investigate the nonlinear evolution of the streaming kink mode as well. Interestingly, some hybrid simulations with a low density plasma in the lobe have suggested the presence of a streaming kink-like structure in the reconnection jet [*Lottermoser et al.*, 1998; *Arzner and Scholer*, 2001; *Higashimori and Hoshino*, 2012; *Liu et al.*, 2012]. However, since the lobe densities in these simulations are still higher than that in the earth’s magnetotail, we expect that a streaming kink-like structure can be excited easily in more realistic situations.

In this paper, we have only discussed the linear stability of the streaming MHD instability for an isotropic pressure, i.e.,  $p_{\parallel} = p_{\perp}$ ; however, under a collisionless reconnection, it is known that the anisotropy in pressure for  $p_{\parallel} > p_{\perp}$  can be generated [e.g., *Hirabayashi and Hoshino*, 2013]. In this situation, the fire-hose instability may couple with the streaming modes [*Arzner and Scholer*, 2001]. Under the anisotropic plasma situation with  $p_{\parallel} > p_{\perp}$ , the magnetic tension force for the distorted magnetic field line becomes weak; as a result, we may expect that the streaming instability can be easily excited. However, a study of the behavior of an anisotropic plasma is beyond the scope of this paper.

We assumed that the physical quantities were uniform in the  $z$  direction, i.e.,  $\partial/\partial z = 0$ , and that the Fourier modes are restricted to be propagating parallel to the  $x$  direction. However, it would be interesting to understand the oblique propagation as well, because the drifting plasma population parallel to the electric current may couple with the streaming plasma flow. In addition, if there is the density gradient along the plasma flow, the interchange instability may be excited in the  $z$  direction [e.g., *Nakamura et al.*, 2002; *Lapenta and Bettarini*, 2011]. The three dimensional behavior of the streaming instability would play an important role on the actual plasma sheet.

We have discussed the streaming tearing, streaming sausage, and streaming kink modes as possible models of generation of MHD turbulence in the earth’s magnetotail. However, the streaming instability may be found in other applications, one of which is the so-called “channel flow”

formed during the magnetorotational instability (MRI) for accretion disks [e.g., *Balbus and Hawley*, 1991]. It is of interest to note that the particle-in-cell simulation results on the MRI by *Hoshino* [2013] show a streaming kink-type channel flow occurring just before the onset of reconnection. The streaming kink mode may also play an important role on the mass and angular momentum transport during the formation of an accretion disk.

**Acknowledgments.** This work was supported in part by JSPS Grant-in-Aid for Scientific Research (KAKENHI) Grant No. 25287151. The data for this paper are available on request (hoshino@eps.s.u-tokyo.ac.jp).

## References

- Arzner, K., and M. Scholer (2001), Kinetic structure of the post plasmoid plasma sheet during magnetotail reconnection, *J. Geophys. Res.*, , *106*, 3827–3844, doi:10.1029/2000JA000179.
- Asano, Y., T. Mukai, M. Hoshino, Y. Saito, H. Hayakawa, and T. Nagai (2003), Evolution of the thin current sheet in a sub-storm observed by Geotail, *Journal of Geophysical Research (Space Physics)*, *108*, 1189, doi:10.1029/2002JA009785.
- Balbus, S. A., and J. F. Hawley (1991), A powerful local shear instability in weakly magnetized disks. I - Linear analysis. II - Nonlinear evolution, *Astrophys. J.*, , *376*, 214–233, doi:10.1086/170270.
- Bauer, T. M., W. Baumjohann, R. A. Treumann, N. Sckopke, and H. Lühr (1995), Low-frequency waves in the near-Earth plasma sheet, *J. Geophys. Res.*, , *100*, 9605–9618, doi:10.1029/95JA00136.
- Bhattacharjee, A., Y.-M. Huang, H. Yang, and B. Rogers (2009), Fast reconnection in high-Lundquist-number plasmas due to the plasmoid instability, *Physics of Plasmas*, *16*(11), 112,102, doi:10.1063/1.3264103.
- Birn, J., A. V. Artemyev, D. N. Baker, M. Echim, M. Hoshino, and L. M. Zelenyi (2012), Particle Acceleration in the Magnetotail and Aurora, *Space Science Reviews*, *173*, 49–102, doi:10.1007/s11214-012-9874-4.
- Biskamp, D., E. Schwarz, and A. Zeiler (1998), Instability of a magnetized plasma jet, *Physics of Plasmas*, *5*, 2485–2488, doi:10.1063/1.872931.
- Borovsky, J. E., and H. O. Funsten (2003), MHD turbulence in the Earth's plasma sheet: Dynamics, dissipation, and driving, *Journal of Geophysical Research (Space Physics)*, *108*, 1284, doi:10.1029/2002JA009625.
- Borovsky, J. E., R. C. Elphic, H. O. Funsten, and M. F. Thomsen (1997), The Earth's plasma sheet as a laboratory for flow turbulence in high-[beta] MHD, *Journal of Plasma Physics*, *57*, 1–34, doi:10.1017/S0022377896005259.
- Cowley, S. W. H. (1981), Magnetospheric asymmetries associated with the y-component of the IMF, *Planetary and Space Sci.*, *29*, 79–96, doi:10.1016/0032-0633(81)90141-0.
- Fujimoto, K. (2011), Dissipation mechanism in 3D magnetic reconnection, *Physics of Plasmas*, *18*(11), 11206, doi:10.1063/1.3642609.
- Furth, H. P., J. Killeen, and M. N. Rosenbluth (1963), Finite-Resistivity Instabilities of a Sheet Pinch, *Physics of Fluids*, *6*, 459–484, doi:10.1063/1.1706761.
- Gary, S. P. (1991), Electromagnetic ion/ion instabilities and their consequences in space plasmas - A review, *Space Science Reviews*, *56*, 373–415, doi:10.1007/BF00196632.
- Greco, A., A. L. Taktakishvili, G. Zimbardo, P. Veltri, and L. M. Zelenyi (2002), Ion dynamics in the near-Earth magnetotail: Magnetic turbulence versus normal component of the average magnetic field, *Journal of Geophysical Research (Space Physics)*, *107*, 1267, doi:10.1029/2002JA009270.
- Grigorenko, E. E., L. M. Zelenyi, M. S. Dolgonosov, A. V. Artemiev, C. J. Owen, J.-A. Sauvaud, M. Hoshino, and M. Hirai (2011), Non-adiabatic Ion Acceleration in the Earth Magnetotail and Its Various Manifestations in the Plasma Sheet Boundary Layer, *Space Science Reviews*, *164*, 133–181, doi:10.1007/s11214-011-9858-9.
- Higashimori, K., and M. Hoshino (2012), The relation between ion temperature anisotropy and formation of slow shocks in collisionless magnetic reconnection, *Journal of Geophysical Research (Space Physics)*, *117*, A01220, doi:10.1029/2011JA016817.
- Higashimori, K., N. Yokoi, and M. Hoshino (2013), Explosive Turbulent Magnetic Reconnection, *Physical Review Letters*, *110*(25), 255001, doi:10.1103/PhysRevLett.110.255001.
- Hirabayashi, K., and M. Hoshino (2013), Magnetic reconnection under anisotropic magnetohydrodynamic approximation, *Physics of Plasmas*, *20*(11), 112111, doi:10.1063/1.4831754.
- Hoshino, M. (1991), Forced magnetic reconnection in a plasma sheet with localized resistivity profile excited by lower hybrid drift type instability, *J. Geophys. Res.*, , *96*, 11,555, doi:10.1029/91JA00984.
- Hoshino, M. (2013), Particle Acceleration during Magnetorotational Instability in a Collisionless Accretion Disk, *Astrophys. J.*, , *773*, 118, doi:10.1088/0004-637X/773/2/118.
- Hoshino, M., A. Nishida, T. Yamamoto, and S. Kokubun (1994), Turbulent magnetic field in the distant magnetotail: Bottom-up process of plasmoid formation?, *Geophys. Res. Lett.*, , *21*, 2935–2938, doi:10.1029/94GL02094.
- Hoshino, M., T. Mukai, T. Yamamoto, and S. Kokubun (1998), Ion dynamics in magnetic reconnection: Comparison between numerical simulation and Geotail observations, *J. Geophys. Res.*, , *103*, 4509–4530, doi:10.1029/97JA01785.
- Hoshino, M., T. Mukai, T. Terasawa, and I. Shinohara (2001), Suprathermal electron acceleration in magnetic reconnection, *J. Geophys. Res.*, , *106*, 25,979–25,998, doi:10.1029/2001JA900052.
- Ishisaka, K., T. Okada, K. Tsuruda, H. Hayakawa, T. Mukai, and H. Matsumoto (2001), Relationship between the Geotail spacecraft potential and the magnetospheric electron number density including the distant tail regions, *J. Geophys. Res.*, , *106*, 6309–6320, doi:10.1029/2000JA000077.
- Krauss-Varban, D., and N. Omid (1995), Large-scale hybrid simulations of the magnetotail during reconnection, *Geophys. Res. Lett.*, , *22*, 3271–3274, doi:10.1029/95GL03414.
- Lapenta, G., and L. Bettarini (2011), Self-consistent seeding of the interchange instability in dipolarization fronts, *Geophys. Res. Lett.*, , *38*, L11102, doi:10.1029/2011GL047742.
- Lazarian, A., and E. T. Vishniac (1999), Reconnection in a Weakly Stochastic Field, *Astrophys. J.*, , *517*, 700–718, doi:10.1086/307233.
- Lazarian, A., L. Vlahos, G. Kowal, H. Yan, A. Beresnyak, and E. M. de Gouveia Dal Pino (2012), Turbulence, Magnetic Reconnection in Turbulent Fluids and Energetic Particle Acceleration, *Space Science Reviews*, *173*, 557–622, doi:10.1007/s11214-012-9936-7.
- Lee, L. C., S. Wang, C. Q. Wei, and B. T. Tsurutani (1988), Streaming sausage, kink and tearing instabilities in a current sheet with applications to the earth's magnetotail, *J. Geophys. Res.*, , *93*, 7354–7365, doi:10.1029/JA093iA07p07354.
- Liu, Y.-H., J. F. Drake, and M. Swisdak (2012), The structure of the magnetic reconnection exhaust boundary, *Physics of Plasmas*, *19*(2), 022,110, doi:10.1063/1.3685755.
- Lottermoser, R.-F., M. Scholer, and A. P. Matthews (1998), Ion kinetic effects in magnetic reconnection: Hybrid simulations, *J. Geophys. Res.*, , *103*, 4547–4560, doi:10.1029/97JA01872.
- Loureiro, N. F., A. A. Schekochihin, and S. C. Cowley (2007), Instability of current sheets and formation of plasmoid chains, *Physics of Plasmas*, *14*(10), 100,703, doi:10.1063/1.2783986.
- Loureiro, N. F., D. A. Uzdensky, A. A. Schekochihin, S. C. Cowley, and T. A. Yousef (2009), Turbulent magnetic reconnection in two dimensions, *Mon. Not. R. Astron. Soc.*, , *399*, L146–L150, doi:10.1111/j.1745-3933.2009.00742.x.
- Matthaeus, W. H., and S. L. Lamkin (1986), Turbulent magnetic reconnection, *Physics of Fluids*, *29*, 2513–2534, doi:10.1063/1.866004.
- Miura, A., and P. L. Pritchett (1982), Nonlocal stability analysis of the MHD Kelvin-Helmholtz instability in a compressible plasma, *J. Geophys. Res.*, , *87*, 7431–7444, doi:10.1029/JA087iA09p07431.
- Nakamura, M. S., H. Matsumoto, and M. Fujimoto (2002), Interchange instability at the leading part of reconnection jets, *Geophys. Res. Lett.*, , *29*, 1247, doi:10.1029/2001GL013780.
- Nakamura, R. (2006), Substorms and Their Solar Wind Causes, *Space Science Reviews*, *124*, 91–101, doi:10.1007/s11214-006-9131-9.
- Petrukovich, A. A. (2011), Origins of plasma sheet  $B_y$ , *Journal of Geophysical Research (Space Physics)*, *116*, A07217, doi:10.1029/2010JA016386.
- Pritchett, P. L., F. V. Coroniti, and V. K. Decyk (1996), Three-dimensional stability of thin quasi-neutral current sheets, *J. Geophys. Res.*, , *101*, 27,413–27,430, doi:10.1029/96JA02665.
- Pucci, F., and M. Velli (2014), Reconnection of Quasi-singular Current Sheets: The "Ideal" Tearing Mode, *Astrophys. J.*, , *780*, L19, doi:10.1088/2041-8205/780/2/L19.
- Rong, Z. J., W. X. Wan, C. Shen, X. Li, M. W. Dunlop, A. A. Petrukovich, L.-N. Hau, T. L. Zhang, H. Rème, A. M. Du, and E. Lucek (2012), Profile of strong magnetic field  $B_y$  component in magnetotail current sheets, *Journal of Geophysical Research (Space Physics)*, *117*, A06216, doi:10.1029/2011JA017402.
- Russell, C. T. (1972), Noise in the geomagnetic tail, *Planet. Space Sci.*, *20*, 1541–1553, doi:10.1016/0032-0633(72)90055-4.

- Samtaney, R., N. F. Loureiro, D. A. Uzdensky, A. A. Schekochihin, and S. C. Cowley (2009), Formation of Plasmoid Chains in Magnetic Reconnection, *Physical Review Letters*, *103*(10), 105004, doi:10.1103/PhysRevLett.103.105004.
- Sato, T., and R. J. Walker (1982), Magnetotail dynamics excited by the streaming tearing mode, *J. Geophys. Res.*, *87*, 7453–7459, doi:10.1029/JA087iA09p07453.
- Sergeev, V. A., D. G. Mitchell, C. T. Russell, and D. J. Williams (1993), Structure of the tail plasma/current sheet at  $\sim 11 R_E$  and its changes in the course of a substorm, *J. Geophys. Res.*, *98*, 17,345–17,366, doi:10.1029/93JA01151.
- Shigeta, M., T. Sato, and B. Dasgupta (1985), Streaming tearing mode, *Journal of the Physical Society of Japan*, *54*, 3342–3346, doi:10.1143/JPSJ.54.3342.
- Veltri, P., G. Zimbardo, A. L. Taktakishvili, and L. M. Zelenyi (1998), Effect of magnetic turbulence on the ion dynamics in the distant magnetotail, *J. Geophys. Res.*, *103*, 14,897–14,916, doi:10.1029/98JA00211.
- Wang, S., L. C. Lee, and C. Q. Wei (1988), Streaming tearing instability in the current sheet with a super-Alfvénic flow, *Physics of Fluids*, *31*, 1544–1548, doi:10.1063/1.866693.
- Yokoi, N., K. Higashimori, and M. Hoshino (2013), Transport enhancement and suppression in turbulent magnetic reconnection: A self-consistent turbulence model, *Physics of Plasmas*, *20*(12), 122,310, doi:10.1063/1.4851976.
- Zelenyi, L., A. Artemyev, and A. Petrukovich (2014), Properties of Magnetic Field Fluctuations in the Earth’s Magnetotail and Implications for the General Problem of Structure Formation in Hot Plasmas, *Space Science Reviews*, doi:10.1007/s11214-014-0037-7.
- Zelenyi, L. M., A. V. Milovanov, and G. Zimbardo (1998), Multi-scale Magnetic Structure of the Distant Tail: Self-Consistent Fractal Approach, *Washington DC American Geophysical Union Geophysical Monograph Series*, *105*, 321.
- Zelenyi, L. M., S. D. Rybalko, A. V. Artemyev, A. A. Petrukovich, and G. Zimbardo (2011), Charged particle acceleration by intermittent electromagnetic turbulence, *Geophys. Res. Lett.*, *38*, L17110, doi:10.1029/2011GL048983.
- Zenitani, S., and M. Hoshino (2005), Relativistic Particle Acceleration in a Folded Current Sheet, *Astrophys. J.*, *618*, L111–L114, doi:10.1086/427873.
- Zimbardo, G., A. Greco, L. Sorriso-Valvo, S. Perri, Z. Vörös, G. Aburjania, K. Chargazia, and O. Alexandrova (2010), Magnetic Turbulence in the Geospace Environment, *Space Science Reviews*, *156*, 89–134, doi:10.1007/s11214-010-9692-5.

---

Corresponding author: M. Hoshino, Faculty of Science, The University of Tokyo, Tokyo 113-0033, Japan (hoshino@eps.s.u-tokyo.ac.jp)



**Table 1.** Plasma parameters used in our linear analysis: the normalized lobe plasma density  $N_{\text{lobe}} = \rho_{\text{lobe}}/\rho_0$ , the normalized bulk flow speed by the lobe Alfvén speed  $V_{\text{jet}}$ , the normalized wavelength  $k\lambda$ , the ratio of the bulk flow jet size  $\lambda_{\text{jet}}$  and the thickness of the plasma sheet  $\lambda$ , the Hall effect on  $(V_A/\Omega_i)/\lambda$ , and the guide magnetic field  $B_z/B_{\text{lobe}}$ .

Figure	$N_{\text{lobe}}$	$V_{\text{jet}}$	$k\lambda$	$\lambda_{\text{jet}}/\lambda$	Hall	$B_z/B_{\text{lobe}}$
1a	0.01	0.0	0 ~ 2	1.0	0.0	0.0
1b	0.01	0.2	0 ~ 2	1.0	0.0	0.0
1c	0.01	0.4	0 ~ 2	1.0	0.0	0.0
2a	0.01	0.2	0.3	1.0	0.0	0.0
2b	0.01	0.4	1.5	1.0	0.0	0.0
3	0.01	0 ~ 1.5	0 ~ 3.2	1.0	0.0	0.0
4(red, solid)	0.01	0.5	0.3	1.0	0.0	0.0
4(red, dashed)	0.01	0.5	1.0	1.0	0.0	0.0
4(green, solid)	0.01	0.5	1.0	1.0	0.0	0.0
5a	0.01	0 ~ 1.5	0 ~ 3.2	1.0	0.0	0.0
5b	0.05	0 ~ 1.5	0 ~ 3.2	1.0	0.0	0.0
5c	0.1	0 ~ 1.5	0 ~ 3.2	1.0	0.0	0.0
5d	0.1	0 ~ 1.5	0 ~ 3.2	0.5	0.0	0.0
6	0.01	0 ~ 1.5	0 ~ 3.2	1.0	1.0	0.0
7a	0.01	0.0	0.3	1.0	1.0	0.0
7b	0.01	0.2	0.5	1.0	1.0	0.0
7c	0.01	0.4	0.55	1.0	1.0	0.0
8a(blue, solid)	0.05	0.0	0.3	1.0	0.0	0 ~ 1
8b(blue, dashed)	0.05	0.8	0.3	1.0	0.0	0 ~ 1
8c(red, solid/dashed)	0.05	0.8	(1.0/1.5)	1.0	0.0	0 ~ 1
8d(green, solid/dashed)	0.05	0.8	(1.0/1.5)	1.0	0.0	0 ~ 1

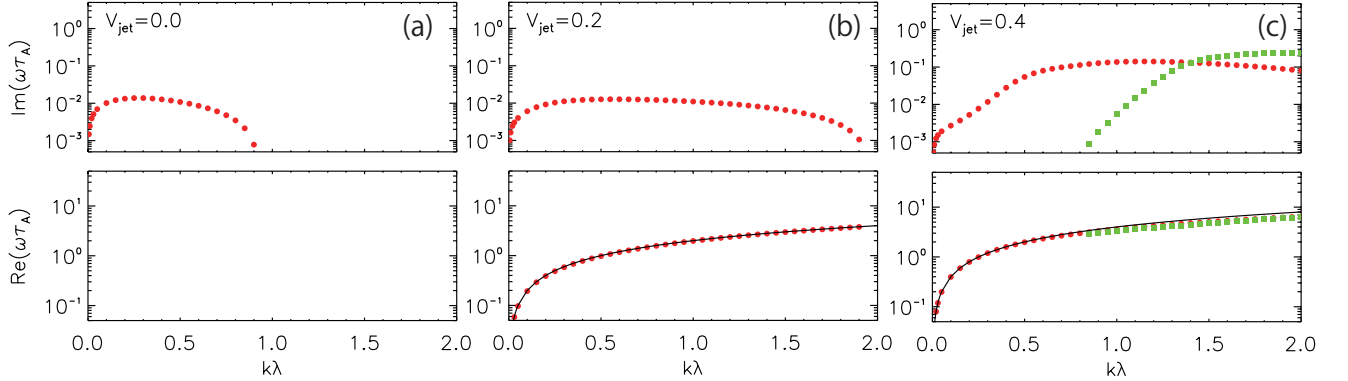


**Figure 1.** Linear growth rate,  $\text{Im}(\omega\tau_A)$ , (top) and oscillation Frequency,  $\text{Re}(\omega\tau_A)$ , (bottom) as the function of wave number,  $k\lambda$ , for three different bulk flow speeds: (a)  $V_{\text{jet}} = v_{\text{jet}}/V_{A,\text{lobe}} = 0$ , i.e., no bulk flow, (b)  $V_{\text{jet}} = 0.2$ , and (c)  $V_{\text{jet}} = 0.4$ . The solid black lines in the bottom panels (b) and (c) are the Doppler shift frequencies of  $\text{Re}(\omega\tau_A) = (k\lambda)V_{\text{jet}}$ .

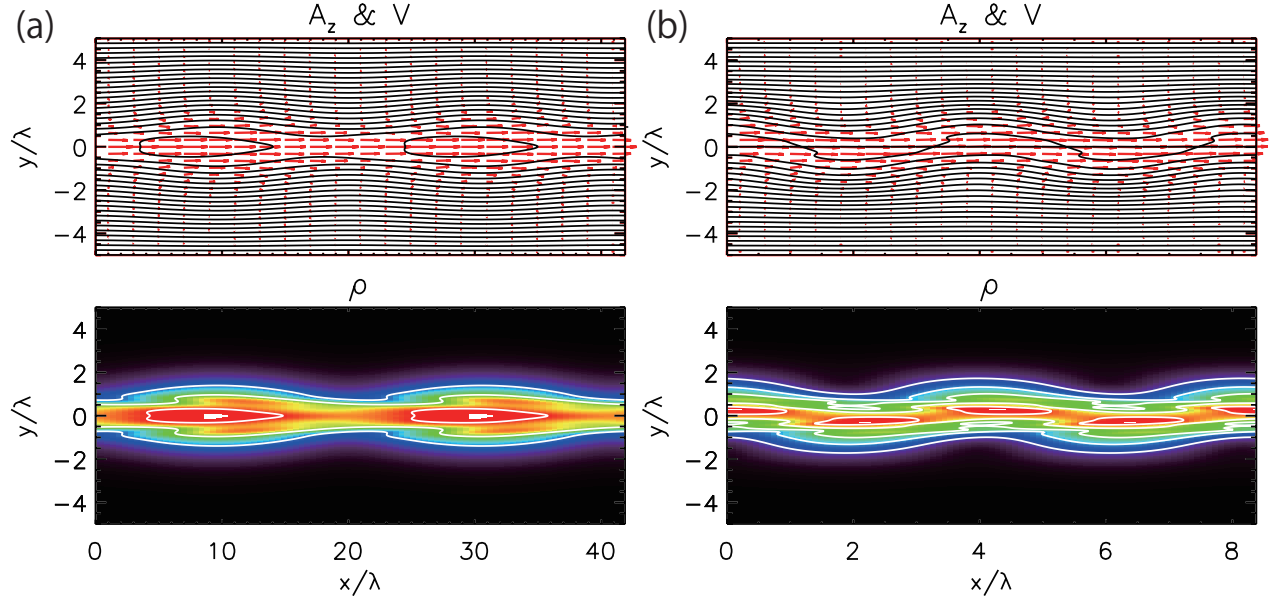


**Figure 2.** Unstable structures for the vector potential,  $A_z$ , (top) and the plasma density,  $\rho$ , (bottom), which were reconstructed from the eigenfunctions and eigenvalues. The flow vectors (red-colored arrows) are superposed on the magnetic field lines (black) of the contours for  $A_z$ . (a) The streaming tearing mode with  $V_{jet} = 0.2$  and  $k\lambda = 0.3$  in Figure 1b, and (b) the streaming kink mode with  $V_{jet} = 0.4$  and  $k\lambda = 1.5$  in Figure 1c.

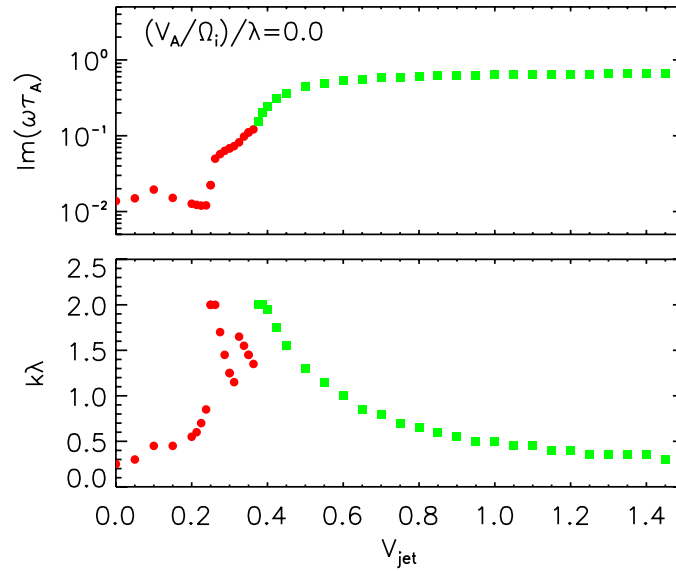


**Figure 3.** Maximum growth rate (top) and the corresponding wave number (bottom) as a function of the bulk flow speed,  $V_{jet}$ , for  $(V_A/\Omega_i)/\lambda = 0$  without a Hall effect. The red-colored circles and the green-colored squares show the symmetric and asymmetric density perturbations, respectively.

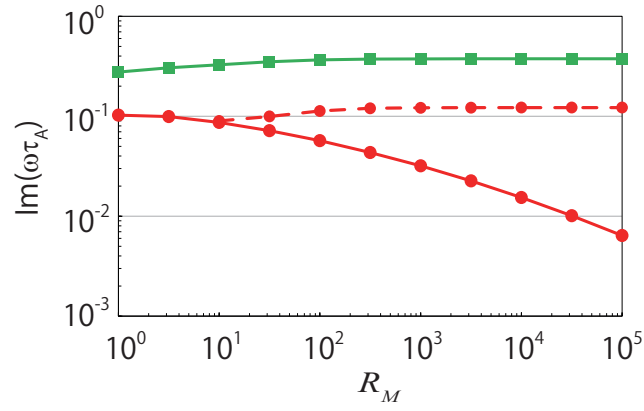


**Figure 4.** Growth rates,  $\text{Im}(\omega\tau_A)$ , for the streaming tearing mode for  $k\lambda = 0.3$  (red-colored solid line with circles), the streaming sausage mode for  $k\lambda = 1.0$  (red-colored dashed line with circles), and the streaming kink mode for  $k\lambda = 1.0$  (green-colored solid line with squares) as a function of magnetic Reynolds number,  $R_M$ . The bulk flow speed was set to be  $V_{\text{jet}} = 0.5$  for all modes.

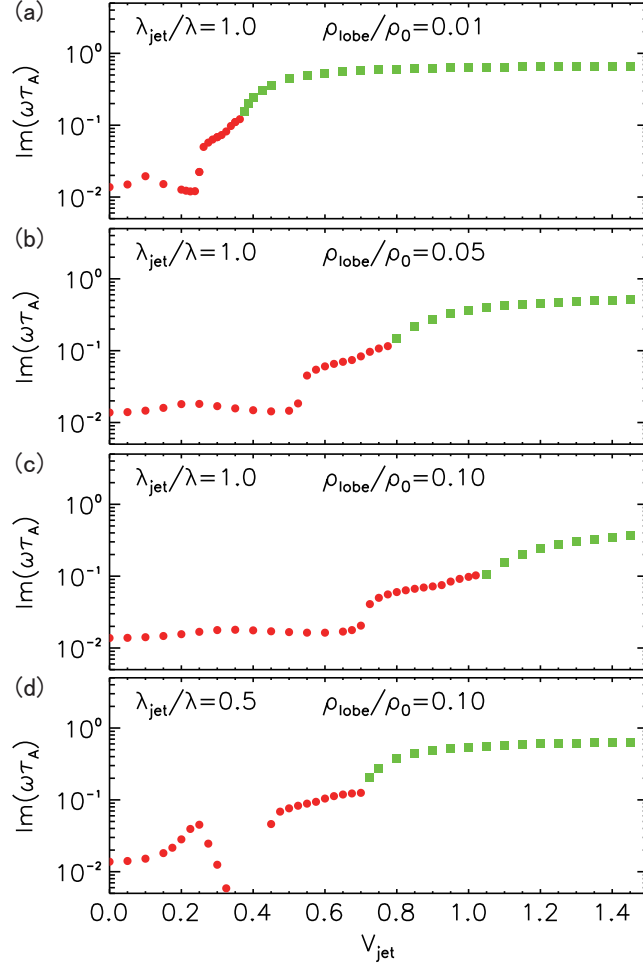


**Figure 5.** Dependence of the lobe plasma density,  $\rho_{\text{lobe}}/\rho_{\text{ps}}$ , and the bulk flow size,  $\lambda_{\text{jet}}$ . Maximum growth rates,  $\text{Im}(\omega\tau_A)$ , are shown as a function of the bulk flow speed,  $V_{\text{jet}}$ , for the following cases: (a)  $\rho_{\text{lobe}}/\rho_0 = 0.01$ ; (b)  $\rho_{\text{lobe}}/\rho_0 = 0.05$ ; and (c)  $\rho_{\text{lobe}}/\rho_0 = 0.1$ . (d) The lobe density is the same as in case (c), but the thickness of the bulk flow jet is narrower, with  $\lambda_{\text{jet}}/\lambda = 0.5$ . The red-colored circles and the green-colored squares show the symmetric (tearing/sausage) and asymmetric (kink) density perturbations, respectively.

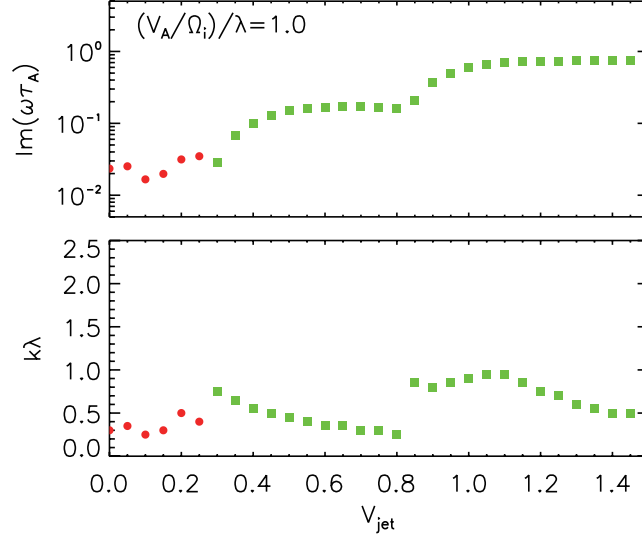


**Figure 6.** Maximum growth rate (top) and its corresponding wave number (bottom) are shown as a function of the bulk flow speed, under the Hall effect with  $(V_A/\Omega_i)/\lambda = 1$ . Except for the Hall parameter, the other parameters are the same as those used in Figure 3.

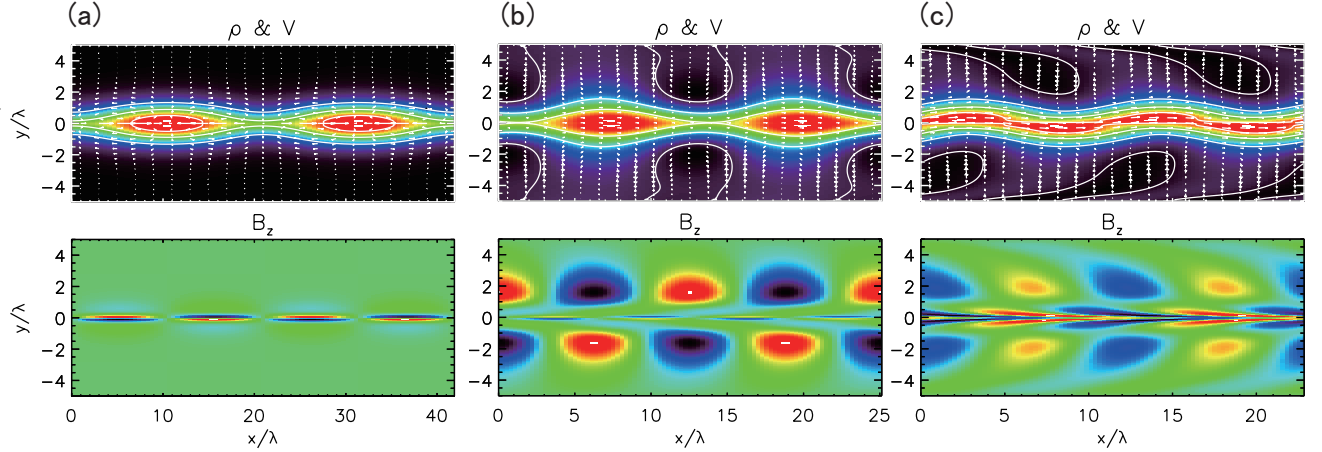


**Figure 7.** Unstable structures for the plasma density,  $\rho$ , (top), the flow vectors,  $\vec{v}$ , (white arrows), and the magnetic field  $B_z$  (bottom): (a) the standard tearing mode without a bulk flow speed  $V_{\text{jet}} = 0$  and  $k\lambda = 0.3$ ; (b) the streaming sausage mode with  $V_{\text{jet}} = 0.2$  and  $k\lambda = 0.5$ ; and (c) the streaming kink mode with  $V_{\text{jet}} = 0.4$  and  $k\lambda = 0.55$ .

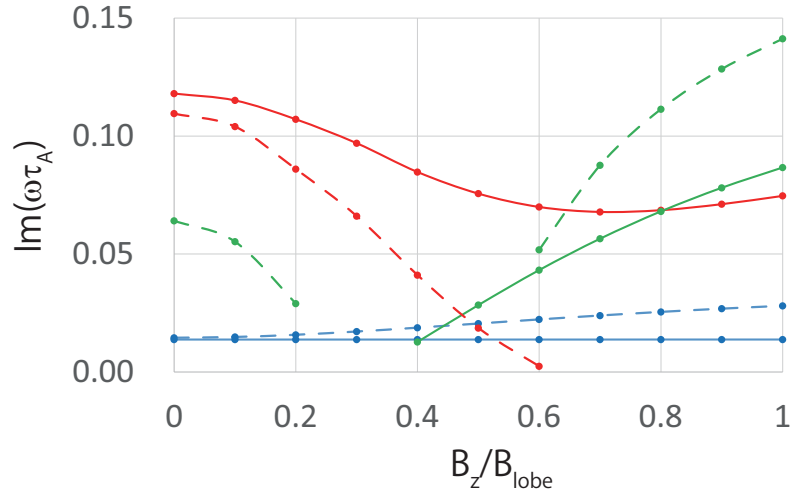


**Figure 8.** Growth rates as a function of the guide magnetic field for four different unstable modes: (a) the standard tearing mode with  $(k\lambda, V_{\text{jet}}) = (0.3, 0)$  (blue and solid line), (b) the streaming tearing mode with  $(k\lambda, V_{\text{jet}}) = (0.3, 0.8)$  (blue and dashed line), (c) the streaming sausage mode with  $(k\lambda, V_{\text{jet}}) = (1.0, 0.8)$  (red and solid line) and with  $(k\lambda, V_{\text{jet}}) = (1.5, 0.8)$  (red and dashed line), and (d) the streaming kink mode with  $(k\lambda, V_{\text{jet}}) = (1.0, 0.8)$  (green and solid line) and with  $(k\lambda, V_{\text{jet}}) = (1.5, 0.8)$  (green and dashed line).